ADVANCING EARTH AND SPACE SCIENCE

JGR Biogeosciences

RESEARCH ARTICLE
10.1029/2020JG006100

Key Points:
- SMAP L4C provides an estimated daily, global terrestrial carbon budget including surface (0- to 5-cm depth) soil organic carbon (SOC)
- L4C SOC is consistent with other global benchmarks including soil inventory records and dynamic global vegetation models ($r > 0.89$)
- SMAP L-band soil moisture has greatest influence on SOC variability in semiarid lands, which encompass about 60% of the global domain

Supporting Information:
- Supporting Information S1

Correspondence to:
K. A. Endsley,
arthur.endsley@ntsg.umt.edu

Citation:
Endsley, K. A., Kimball, J. S., Reichle, R. H., & Watts, J. D. (2020). Satellite monitoring of global surface soil organic carbon dynamics using the SMAP Level 4 Carbon product. *Journal of Geophysical Research: Biogeosciences*, *125*, e2020JG006100. https://doi.org/10.1029/2020JG006100

Received 5 OCT 2020
Accepted 23 NOV 2020
Accepted article online 2 DEC 2020

Satellite Monitoring of Global Surface Soil Organic Carbon Dynamics Using the SMAP Level 4 Carbon Product

K. Arthur Endsley[1], John S. Kimball[1], Rolf H. Reichle[2], and Jennifer D. Watts[3]

[1]Numerical Terradynamic Simulation Group (NTSG), WA Franke College of Forestry and Conservation, University of Montana, Missoula, MT, USA, [2]NASA Global Modeling and Assimilation Office, Goddard Space Flight Center, Greenbelt, MD, USA, [3]Woodwell Climate Research Center, Falmouth, MA, USA

Abstract Soil organic carbon (SOC) is an important metric of soil health and the terrestrial carbon balance. Short-term climate variations affect SOC through changes in temperature and moisture, which control vegetation growth and soil decomposition. We evaluated a satellite data-driven carbon model, operating under the NASA Soil Moisture Active-Passive (SMAP) mission, as a means of monitoring global surface SOC dynamics. The SMAP Level 4 Carbon (L4C) product estimates a daily global carbon budget including surface (0- to 5-cm depth) SOC. We found that the L4C mean latitudinal SOC distribution is generally consistent with alternative assessments from static soil inventory records and dynamic global vegetation models ($r \geq 0.89$). Within forest systems, based on inventory data, L4C SOC is most similar in magnitude to litterfall but is correlated with coarse woody debris ($r = 0.86$) and total SOC ($r = 0.81$). L4C SOC is sensitive to seasonal and annual climate variability, with mean residence times that range from 1.5 years in the wet tropics to 17 years in the cold tundra. Incorporating soil moisture retrievals from the SMAP L-band (1.4 GHz) microwave radiometer within the L4C algorithm provides enhanced soil moisture sensitivity under low-to-moderate vegetation cover (<5 kg m^{-2} vegetation water content). The L-band soil moisture had the greatest impact on the L4C carbon budget in semiarid regions, which span almost 60% of the globe and account for substantial variability in the terrestrial carbon sink. The L4C operational product enables prognostic investigations into effects of recent climate trends and anomalies (e.g., droughts and pluvials) on shallow soil carbon dynamics.

Plain Language Summary Healthy soils are important for agriculture, climate-change adaptation, and biodiversity. The most common way that scientists describe soil health is by taking a sample and measuring the amount of soil organic carbon, which is carbon stored in living things like microbes and fungi or that came from once-living things like trees and other plants and is now in the soil. Collecting these samples requires a lot of time and work, which makes it very difficult for scientists to describe the soil health of large areas like countries or continents. Earth-orbiting satellites that measure surface conditions like the temperature and amount of moisture in the soil have been used to inform computer models of how plants and soil change in response to a changing climate. Because satellites can see the entire globe, the computer models they inform have global coverage. We used one such computer model to estimate the amount of soil organic carbon stored in the world's soils. We compared our estimates of soil organic carbon to estimates from other methods and found that they agree very well once we accounted for the different soil depths used. What is particularly new and exciting about using this computer model for this purpose is that we can estimate seasonal and annual changes in soil organic carbon. This allows us to estimate how much soil health is impacted by short-term natural events like droughts or floods.

1. Introduction

Soil carbon (C) is critical for agricultural productivity and the terrestrial carbon balance (Bond-Lamberty et al., 2018; Paustian et al., 2016). Approximately 55–60% of the mass of soil organic matter exists as soil organic carbon (SOC Cagnarini et al., 2019), which is a key soil health metric that governs many of the ecological, physical, and chemical functions of soil (Bünemann et al., 2018; O'Rourke et al., 2015; Stockmann et al., 2015). In addition to plant photosynthesis, the sequestration of atmospheric carbon dioxide (CO_2) as SOC provides a significant global carbon sink, with soils storing about twice as much carbon as is held in the atmosphere (Köchy et al., 2015).

The sensitivity of SOC stocks to near-term climate variability and longer-term warming trends under anthropogenic climate change is highly uncertain (Bradford et al., 2016; Davidson & Janssens, 2006; Todd-Brown et al., 2014; Wieder et al., 2019). Warmer temperatures may increase SOC losses through heightened microbial activity and soil respiration (Crowther et al., 2016; Hicks Pries et al., 2017). However, warmer and longer growing seasons (Euskirchen et al., 2006; Kim et al., 2012; Park et al., 2016) and rising CO_2 levels may also enhance plant productivity and carbon inputs to the soil (Dietzen et al., 2019; Hursh et al., 2017; van Groenigen et al., 2014; Ziegler et al., 2017), potentially offsetting any increases in SOC losses. Low soil moisture conditions reduce both soil respiration rates and rates of plant C inputs to soil (Dietzen et al., 2019; Wu et al., 2011), with the balance of the two determining the net effect on SOC. Although SOC content is generally higher in regions with higher mean annual precipitation (Zhao et al., 2019), declining soil moisture may reduce soil respiration rates enough to counteract the effects of soil warming on SOC (Conant et al., 2004; Schindlbacher et al., 2012). These changes can have lasting effects on total soil C (Borken et al., 2006), with particularly important implications for the earth's largest soil C stocks: high-latitude regions and global peatlands vulnerable to soil warming and drying (Hugelius et al., 2013; Kwon et al., 2019).

Thus, accurate assessments of SOC are critical for monitoring soil health and the global carbon balance (Crowther et al., 2019; Wiesmeier et al., 2019). However, there are few approaches available for regular and consistent global monitoring of SOC (Harden et al., 2018). Here, we evaluate the ability of an operational, satellite data-driven carbon model, based on the NASA Soil Moisture Active-Passive (SMAP) mission, to diagnose the potential vulnerability or resiliency of terrestrial SOC stocks to near-term (seasonal to decadal) climate variability. The SMAP Level-4 Carbon (L4C) product (Jones et al., 2017) estimates a daily global carbon budget, including dynamic changes in surface SOC within the top 5 cm of soil resulting from daily inputs of C from vegetation litterfall and loss of CO_2 from respiration. Launched in 2015, the SMAP mission specifically aims to improve global drought assessment and understanding of the terrestrial water, energy, and carbon cycles and their linkages. The SMAP L-band (1.4 GHz) microwave radiometer is especially sensitive to surface soil moisture variability (Reichle et al., 2017). Soil moisture is a key control for ecosystem productivity and soil respiration (Jung et al., 2017) and is a key constraint on the contribution of semiarid ecosystems to the terrestrial carbon sink (Ahlström et al., 2015).

This paper evaluates the use of SMAP L4C modeled surface SOC stocks as a means of monitoring spatial and temporal variations in global soil C sequestration. A guiding premise for this work is that SOC within the surface soil layer is a sensitive environmental indicator of the potential vulnerability or resiliency of terrestrial carbon stocks to near-term (seasonal to decadal) climate variability, through the interaction of this variability with the plant-soil system (Bond-Lamberty et al., 2018; Pugnaire et al., 2019; Zhao et al., 2019). Unlike other components of the terrestrial carbon budget, the SOC metric reflects the integrated ecosystem response to climate-related impacts on vegetation net primary productivity and heterotrophic respiration. Compared to static SOC inventories, SMAP L4C provides a dynamic, global estimate of surface SOC integrated within a daily carbon budget that quantifies vegetation, soil moisture, and soil temperature-related controls on the accumulation and decomposition of SOC (Jones et al., 2017). Here, we used the SMAP L4C product to (1) quantify the impact of the SMAP L-band brightness temperature (Tb) observations on the L4C SOC estimates relative to model estimates derived without incorporating SMAP observations; (2) verify the internal logic of SOC dynamics within L4C and validate L4C SOC estimates against multiple, independent, global, or regional SOC records derived from soil inventories or other model-based assessments; and (3) assess patterns in global, surface SOC magnitudes, and mean residence times (MRTs) and their relationships to biome types and recent climate variability.

2. Methods

2.1. Data Sources

2.1.1. SMAP L4C Surface SOC

The SMAP mission produces a set of operational global land data products, including (Level 1) microwave brightness temperature (Tb) observations, (Levels 2 and 3) surface soil moisture retrievals, and model-enhanced (Level 4) estimates of surface (0- to 5-cm depth) and root-zone (0- to 1-m depth) soil moisture and temperature (Reichle et al., 2017), along with a daily carbon budget. The SMAP L4C product provides continuous, global, daily estimates of net ecosystem CO_2 exchange at 9-km resolution (Jones et al., 2017). The L4C algorithm incorporates vegetation observations from the Moderate Resolution Imaging Spectroradiometer (MODIS) and SMAP daily soil temperature and surface and root-zone

soil moisture information as key environmental drivers for estimating ecosystem productivity, respiration, and SOC.

The L4C algorithm combines a light-use efficiency model for estimating vegetation gross primary production (GPP) with a three-pool soil decomposition and heterotrophic respiration (RH) model with first-order kinetics (Jones et al., 2017). Soil temperature and soil moisture at the root zone and surface are derived from the SMAP Level 4 Soil Moisture (L4SM) product (Reichle et al., 2017, 2019) and are used to constrain the GPP and soil RH estimates. Meteorological drivers include daily minimum air temperature, atmospheric vapor pressure deficit, and photosynthetically active radiation (PAR), all of which potentially constrain GPP; these drivers are derived from the Goddard Earth Observing System 5 Forward Processing system (GEOS-5 FP; Lucchesi, 2018). The fraction of PAR intercepted by the vegetation canopy (fPAR) is derived from the MODIS MOD15A2 (Collection 6) product. The global distribution of plant functional type (PFT) classes are defined from the MODIS MOD12Q1 (Type 5) land-cover classification, which distinguishes up to 8 global PFT classes (Friedl et al., 2010): Evergreen Needleleaf and Broadleaf forest, Deciduous Needleleaf and Broadleaf forest, Shrub, Grass, Cereal Crops, and Broadleaf Crops (Figure S1).

The L4C algorithm is calibrated separately for each PFT class using CO_2 flux observations from a global network of eddy covariance towers (Baldocchi, 2008). Net ecosystem CO_2 exchange (NEE) is derived as the daily residual difference between vegetation net primary production (NPP, which is GPP minus plant CO_2 respiration) and RH, where plant CO_2 respiration (autotrophic respiration) is derived as a PFT-specific fraction of GPP. This is based on the assumption that carbon-use efficiency, which describes how much GPP remains after autotrophic respiration (the NPP:GPP ratio), varies conservatively within individual PFT classes. Linear ramp functions, calculated separately for each PFT, define the change in CO_2 flux where there is an estimated reduction of GPP and RH under less favorable environmental conditions, including soil moisture deficits or cold temperatures. These functions are defined by two parameters, the lower and upper bounds on each environmental condition (e.g., X% soil moisture). When conditions fall below the lower bound, GPP or RH are completely constrained (i.e., multiplier is 0); above the bound, they are unconstrained (i.e., multiplier is 1) and values in between are a linear interpolation between 0 and 1. Soil temperature is an exception, where the multiplier on RH is defined by an Arrhenius function instead (Jones et al., 2017).

During L4C operations, a constant daily fraction of estimated NPP is allocated as litterfall input to SOC storage in three pools with cascading litter quality and progressively slower decay rates. The first of these SOC pools, metabolic SOC, consists of labile plant C inputs (e.g., leaves and fine roots with low carbon-to-nitrogen, or C:N, ratios). The remainder of the litter that does not enter the metabolic SOC pool enters the structural SOC pool, which consists of coarse woody debris and roots with moderate C:N ratio and high lignin content. A fraction of the structural SOC pool is transferred to the third pool, recalcitrant SOC, characterized by high C:N, tannins, phenols, and other less labile compounds (Jones et al., 2017).

RH is calculated daily as the sum of heterotrophic respiration from each pool according to a decay rate constrained by limiting environmental conditions. Prior to the SMAP mission launch in 2015, the L4C SOC pools were initialized to steady-state conditions using long-term (2000-2015) climatologies of mean daily fractional photosynthetic vegetation cover from the MODIS fPAR record, of L4SM soil moisture and temperature, and of daily surface meteorology from the Modern Era Retrospective Re-analysis (MERRA-2, Gelaro et al., 2017); these conditions inform an analytical solution to the differential equations that govern daily change in SOC (Jones et al., 2017). This approach brings the SOC pools as close as possible to the steady state prior to the SMAP mission launch, whereupon NPP litterfall and daily RH, subject to environmental conditions, govern change in each pool. Real-world SOC pools may not be in equilibrium and this presents a challenge for inferring trends in SOC pools. However, the use of observed, contemporary (2000-2017) RH fluxes to calibrate L4C gives us confidence in the magnitude of the SOC stock required to sustain the observed RH flux.

The complete carbon budget in L4C is calculated at 1-km resolution, similar to the spatial scale of the MODIS vegetation inputs. Daily model outputs are posted to a coarser 9-km global EASE-Grid 2.0 format (Brodzik et al., 2012) consistent with the SMAP L4SM product, while preserving subgrid PFT means within each 9-km grid cell. Thus, spatial mean values for SOC and other components of the daily carbon budget are recorded for each 9-km grid cell and up to eight individual PFT classes within each cell, based on the 1-km MODIS PFT map. This nested structure enables partial reconstruction of the finer 1-km pattern in L4C outputs, including SOC (Figure 1).

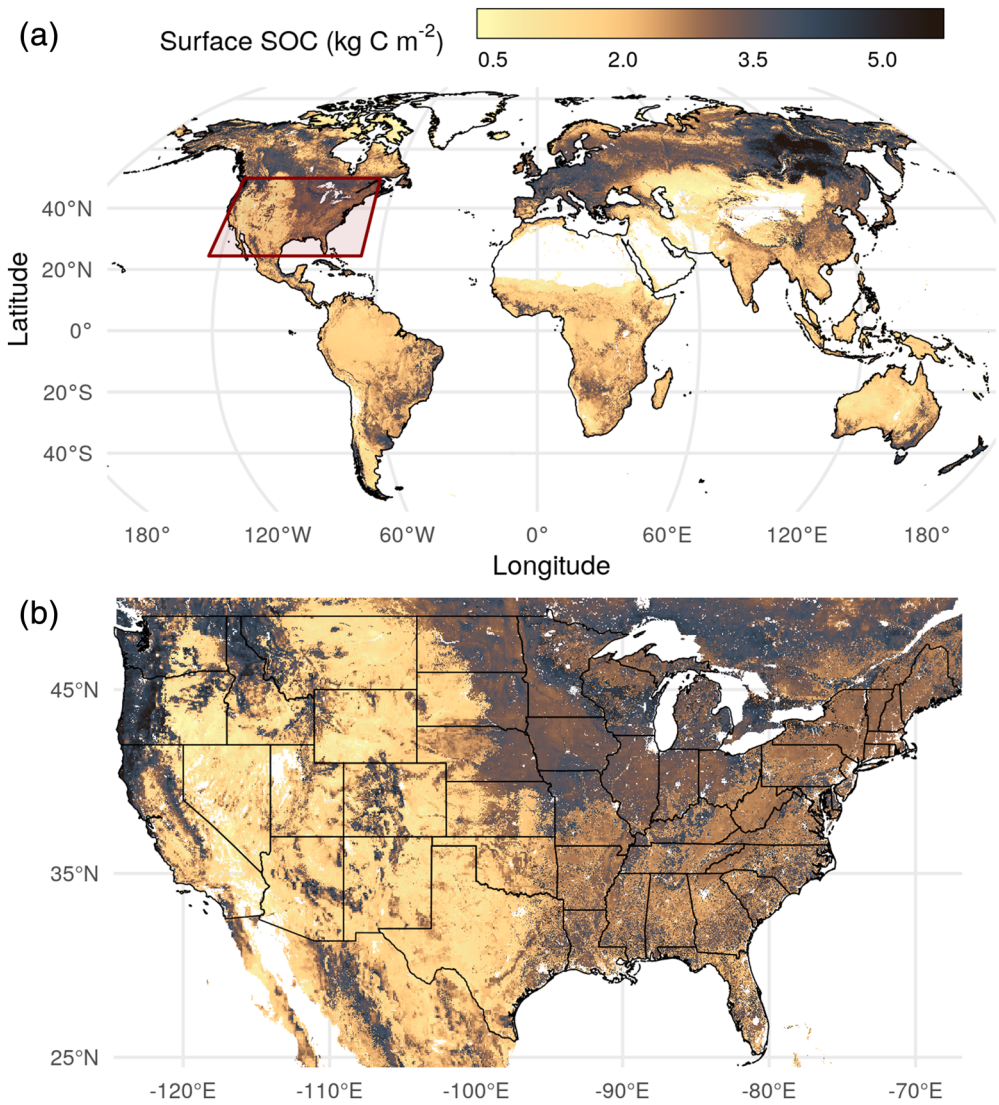

Figure 1. Global map of mean, surface soil organic carbon (SOC) at 9-km scale in 2016 from L4C (a) and down-scaled 1-km surface SOC (b) for the same year over the contiguous United States (CONUS), with state boundaries as black lines. Inset area (b) is outlined in red in the top figure (a). The color ramp is clipped to the 1st and 99th percentiles across the globe.

Soil moisture at the root zone and near the surface is key controls on GPP and RH, respectively, in the L4C model. The SMAP L4SM product assimilates SMAP Tb observations into the GEOS-5 Catchment land model to produce continuous (3-hourly), global gridded estimates of surface and root-zone soil moisture and temperatures (Reichle et al., 2019). Under low-to-moderate vegetation biomass cover (<5 kg m^{-2} vegetation water content), the L-band (1.4 GHz) Tb observations are especially sensitive to the dielectric properties, including moisture levels, within the surface soil layer (Entekhabi et al., 2010), which is congruent with the 0- to 5-cm surface soil layer depth of the SMAP L4SM product. This is also consistent with the L4C calibration against flux tower observations, as the surface soil layer generally encompasses more recent and labile SOC, which generally contributes the largest component of the soil RH flux (Bond-Lamberty et al., 2004) and is more sensitive to seasonal and interannual climate variability (Cagnarini et al., 2019; Chen et al., 2013) relative to deeper soil layers. The accuracy of L4SM soil moisture estimates is lower in areas of dense vegetation and areas where precipitation gauge measurements are sparse (Reichle et al., 2017), due to uncertainty in the Tb assimilation and the Catchment land model, respectively. In these areas, we expect that the surface soil moisture constraint on RH, in particular, is less reliable and, in turn, surface SOC dynamics

more uncertain. As the spatial distribution of the SOC stock is determined by the long-term soil moisture and soil temperature climatologies, SOC stock size is less impacted by this uncertainty.

2.1.2. SMAP L4C Diagnostic Products

The SMAP operational L4C product (L4C Ops Version 4), described above, extends from 31 March 2015 to present and is publicly distributed through the National Snow and Ice Data Center (NSIDC). For this study, we conducted alternative simulations from two other L4C variants to provide model diagnostic and sensitivity assessments.

First, we used a model-only or "Nature Run" variant of L4C derived using daily soil moisture and temperature inputs from a model-only Nature Run of the L4SM algorithm and using MERRA-2 surface meteorology inputs (Endsley et al., 2020). The L4C Nature Run is not informed by SMAP Tb observations and provides an extended data record from 1 January 2000 through the end of 2017. Second, we used the L4C "Open Loop," which uses the model-only estimates of soil moisture and soil temperature from the L4SM Nature Run, but the same surface meteorological drivers as L4C Ops. The resulting difference between L4C Ops and Open Loop simulations quantifies the impact of SMAP Tb observations on the daily carbon budget components, including SOC.

The difference in climatology between L4C Ops (v4) and the L4C Nature Run (v7.2) is mitigated by an affine statistical transformation where rank-sorted values from L4C Ops ($y_{i,t}$) are regressed on rank-sorted values from L4C Nature Run ($\hat{y}_{i,t}$) for each pixel i, where t denotes time.

$$y_{i,t} = \alpha_i + \beta_i \hat{y}_{i,t} + \varepsilon_{i,t} \tag{1}$$

This adjustment mitigates potential bias differences between the two product versions, which can confound the consistent estimation of L4C anomalies and trends. The coefficients α_i and β_i are estimated from a training set where the two versions overlap, 31 March 2015 through the end of 2017, and then applied to adjust the values in the Nature Run for the period from 1 January 2000 through 31 March 2015 so as to better match the mean and variance in L4C Ops.

As surface SOC is a dynamic quantity, we conducted time series analyses on the detrended anomalies of the model output monthly means. Piecewise linear regression on the monthly means, $y_{i,t}$, was used to derive detrended anomalies for each pixel i and year t (Equation 2), where detrended anomalies correspond to the residuals of the linear regression. A knot, k, at the tie point (April 2015) between the L4C Nature Run and L4C Ops time series was included to allow for a possible change in trend. The linear regression was applied separately for each calendar month (January through December) so that the resulting anomalies have no trend and zero mean within a given calendar month (e.g., January).

$$y_{i,t} = \beta_0 + \beta_1(t) + \beta_2 \left[\max\,(0, t-k)\right] + \varepsilon_{i,t} \text{ where } \varepsilon_{i,t} \in \mathbf{N}(0, \sigma^2) \tag{2}$$

The impact of SMAP Tb observations and the downstream L4SM soil moisture and temperature estimates on the L4C outputs was quantified as the root mean-squared difference (RMSD) between the L4C Ops and L4C Open Loop products. The climate aridity index, defined as the precipitation-to-potential evapotranspiration (PET) ratio, was used to explore the impact of SMAP Tb on the estimated carbon budget in semiarid regions, which we define as regions where this ratio is less than one. To this end, mean annual, temperature, precipitation, and PET for the 2011–2018 period were derived from the Climatic Research Unit (CRU) TS4.03 data set (Harris et al., 2014), which provides monthly meteorological fields for the globe at 0.5° resolution.

2.1.3. Alternative Products for L4C Assessment

In order to validate the spatial distribution and stock size of surface SOC as modeled by L4C, we compared the L4C estimates to other inventory- or model-based products. SoilGrids-250 m (Hengl et al., 2017) is a machine learning-based model of inventory data that extrapolates SOC and other edaphic variables at 250-m scale across the globe. It is vertically differentiated, with soil layers at 5, 15, 30, 60, 100, and 200 cm. SOC in the 0- to 5-cm layer was selected from SoilGrids-250 m for evaluating the L4C surface SOC results. However, unlike L4C, the SoilGrids-250 m product (hereafter, "SoilGrids") represents a static average of recent soil conditions.

The Global Soil Dataset for use in Earth System Models (GSDE Shangguan et al., 2014) and the World Inventory of Soil property Estimates 30-arcsecond global map of soil properties (WISE30sec Batjes, 2016)

are also based on static soil inventory data. The WISE30sec product expands upon the Harmonized World Soil Database (HWSD FAO, 2009) by adding additional soil profiles, adding climate, and land-use covariates; extending the number and depth of soil layers; and quantifying uncertainty. The GSDE uses the HWSD mapping framework but adds several new soil profiles and decouples soil mapping units from independent classifications, improving the consistency and comparability across multiple international data sources; the GSDE also extends the number and depth of soil layers relative to HWSD, including eight soil layers with a top layer from 0- to 4.5-cm depth. The WISE30sec product has five soil layers with boundaries at 30-, 50-, 100-, 150-, and 200-cm depth.

The Northern Circumpolar Soil Carbon Database, Version 2 (NCSCDv2), is produced in a similar fashion (Hugelius et al., 2014) and has four soil layers with boundaries at 30-, 100-, 200-, and 300-cm depth. In this study, we use the NCSCDv2 polygon data set, which covers the Circumpolar Arctic, a region with a southern boundary that fluctuates in latitude and generally encompasses continuous and discontinuous permafrost regions of the Northern Hemisphere. The Circumpolar Arctic also includes the domain of the NASA Arctic Boreal Vulnerability Experiment (ABoVE), and we compared L4C SOC and RH estimates to corresponding values reported by Huntzinger et al. (2020) for this region.

As an additional regional comparison, for the United States, state-level forest SOC inventories from the USDA Forest Inventory and Analysis (FIA) database (Smith et al., 2014) were also compared to the L4C surface SOC estimates. State-level total forest carbon in dead trees and woody debris, litterfall, and SOC is reported yearly for all U.S. states except Hawaii from 1990 to 2008 as part of the national greenhouse gas inventory. The USDA FIA data are reported at the state level only, which restricts their use in comparison to L4C at finer spatial scales. Instead, we calculated the mean surface SOC values within forest PFT classes from L4C Ops for the 2000–2007 period and then totaled the forest SOC values within each state for comparison with the corresponding 2000–2007 mean state FIA totals for each SOC pool.

In addition to the inventory-based products above, global SOC simulations from the TRENDY ensemble of dynamic global vegetation models or DGVMs (Le Quéré et al., 2018; Sitch et al., 2015) were also compared to the L4C surface SOC estimates. Eight DGVMs and the ensemble mean from the TRENDYv7 "S3" simulations (which include time varying atmospheric CO_2 concentrations, climate, and land use) provided annual SOC and monthly NPP and RH estimates for the globe at 1° resolution. The TRENDYv7 SOC is not vertically differentiated but represents the total organic carbon in soil. For comparison to the other products, which have defined soil layers, we assumed that TRENDYv7 SOC represents, on average, the top 1 m of soil.

All of the gridded products (SoilGrids, GSDE, WISE30sec, and TRENDYv7) were projected onto a consistent 9-km global EASE-Grid 2.0 using bilinear resampling for comparison to L4C. The NCSCDv2 SOC record consists of irregular polygon data; for comparison to L4C across latitude bands, the NCSCDv2 data were rasterized and projected onto the 9-km global EASE-Grid 2.0. The polygons were also intersected with the L4C SOC grid; zonal statistics were then calculated to compare total SOC stock size in the Circumpolar Arctic region. Products were compared across latitude bands, PFT classes, terrestrial ecoregions (Olson et al., 2001), and global TransCom regions (Baker et al., 2006) for summarizing and comparing SOC patterns.

The TRENDYv7 models provide a means for comparing L4C surface SOC dynamics with more sophisticated Earth System Model projections. The TRENDYv7-modeled RH and NPP data were detrended, centered, and scaled in the same way as the L4C variables (Equation 2). For comparison to one another, detrended anomalies from TRENDYv7 and the harmonized L4C Ops and Nature Run 20-year time series were smoothed using a low-pass filter analogous to a moving window average, but with zero phase offset. Window sizes were determined empirically and are different because of the different levels of high-frequency variation in the two fluxes; a 3-month window was used for NPP anomalies and a 5-month window for RH anomalies.

2.2. Derivation of Depth Profiles

Most of the alternative SOC products described above reflect different soil layers than the L4C surface SOC (0–5 cm) definition; therefore, we developed and applied empirical methods for interpolating SOC measurements that span deeper soil layers to that of the top 5 cm, consistent with L4C. We first derived profiles of volumetric (mass per volume) and areal (mass per area) SOC from the vertically differentiated comparison datasets listed above (except GSDE) but also from Jobbágy and Jackson (2000, Table 3), which provided SOC in layers with boundaries at 100-, 200-, and 300-cm depth. SOC in each soil layer was given in mass-per-volume or mass-per-area units in the SoilGrids, NCSCDv2, and Jobbágy and Jackson (2000) data

sets. However, the WISE30sec data set provides SOC as a volume percentage, which was converted to areal SOC (g C m^{-2}) using the following relationship:

$$\mathrm{SOC} = (1 - f_C)(\mathrm{BD} \times \mathrm{SOC}_{\%} \times h). \tag{3}$$

In Equation 3, f_C is the volumetric fraction of coarse fragments, BD is the bulk density (mass per volume), $\mathrm{SOC}_{\%}$ is the SOC content as a volume percentage, and h is the depth of the soil layer in question. For the WISE30sec data set, the coarse fraction, bulk density, and $\mathrm{SOC}_{\%}$ fields were provided for each soil layer and for each mapping unit (a unique set of edaphic, topographic characteristics). We calculated a weighted mean for each field based on the proportional area of each mapping unit to obtain a single coarse fraction, bulk density, and $\mathrm{SOC}_{\%}$ value for each soil layer. Areal SOC values were converted to volumetric SOC using the soil layer depth; natural splines were then fit to the median volumetric SOC in each layer for each data set.

2.3. Sensitivity Analysis

To verify the internal logic of SMAP L4C regarding SOC dynamics, we performed a sensitivity analysis of the detrended anomalies of monthly mean SOC, NPP, and RH over the period from January 2000 through December 2019 (240 months) using the combined L4C Ops and Nature Run data. Change in surface SOC is a function of the balance between C inputs from litterfall (computed as prescribed fraction of NPP) and C losses from soil decomposition and RH. Therefore, detrended anomalies of change in surface SOC (ΔSOC) were regressed on lagged, detrended anomalies in NPP and RH, as shown in Equation 4, where $f()$ is the detrending operation (i.e., the residuals from Equation 2). Successive lags in NPP and RH of ℓ months, from $\ell = 1$ to $\ell = 6$, were used to determine the temporal extent of their influence on ΔSOC. Equation 4 was fit for each pixel using ordinary least squares, yielding β_{NPP} and β_{RH} coefficients for each.

$$f(\Delta\mathrm{SOC}_t) = f\left(\mathrm{SOC}_t - \mathrm{SOC}_{t-1}\right) = \beta_{\mathrm{NPP}} f\left(\mathrm{NPP}_{t-\ell}\right) + \beta_{\mathrm{RH}} f(\mathrm{RH}_{t-\ell}) + \varepsilon_t \tag{4}$$

2.4. Stability of Surface SOC

The MRT of SOC, or the average time a unit mass of carbon is sequestered in the soil before it is respired, serves as a metric of soil carbon sequestration and relative SOC stability under climatic variability (Bloom et al., 2016; Chen et al., 2013). To quantify surface SOC stability in different biomes and across the global domain, we calculated the MRT of the L4C SOC stock as the quotient of mean annual SOC and RH in the years 2016–2019.

3. Results

To evaluate the use of L4C as a means of monitoring spatial and temporal variations in global, surface SOC, we conducted several assessments of the L4C SOC data set, the internal logic of the L4C algorithm, and how L4C SOC compares to alternative SOC data products. First, we quantified the impact of SMAP Tb observations on the L4C carbon budget by comparing the L4C Ops and Open Loop model runs. We then compared the spatial distributions of surface SOC derived from L4C and other products at global and regional scales. Surface SOC in L4C is dynamic, so we also compared changes in the component productivity and respiration fluxes estimated by L4C to an ensemble of DGVMs. Finally, we used a sensitivity analysis to verify the L4C internal SOC dynamics in relation to underlying changes in surface soil moisture and temperature.

3.1. SOC Depth Profiles

The SOC profiles we derived are shown in Figure 2 and are similar to those reported by Burke and Lobell (2017) and Tifafi et al. (2018). The profiles were used to calculate ratios of volumetric SOC in the top 5 cm to volumetric SOC at depth; these ratios indicate that volumetric SOC content at depth is a fraction of that near the surface; however, areal SOC integrates from the surface to the bottom of the soil column; hence, deeper soil layers have higher areal SOC content. As Hobley et al. (2015) anticipated, the depth profile for the NCSCDv2, which is limited to a region with low mean annual temperatures, exhibits the steepest vertical gradient. The uncertainty in SOC content is highest near the surface; the 5- to 100-cm areal SOC content ratios, expressed as percentages, vary across the data sets: 7.0% from Jobbágy and Jackson (2000), 10.0% from NCSCDv2, 12.5% from WISE30sec, and 13.1% for SoilGrids. Excluding the NCSCDv2, which is not globally representative, SoilGrids is the most recently available data set and seems to perform best among diverging estimates in comparison to in situ data (Tifafi et al., 2018). Ratios from SoilGrids and WISE30sec

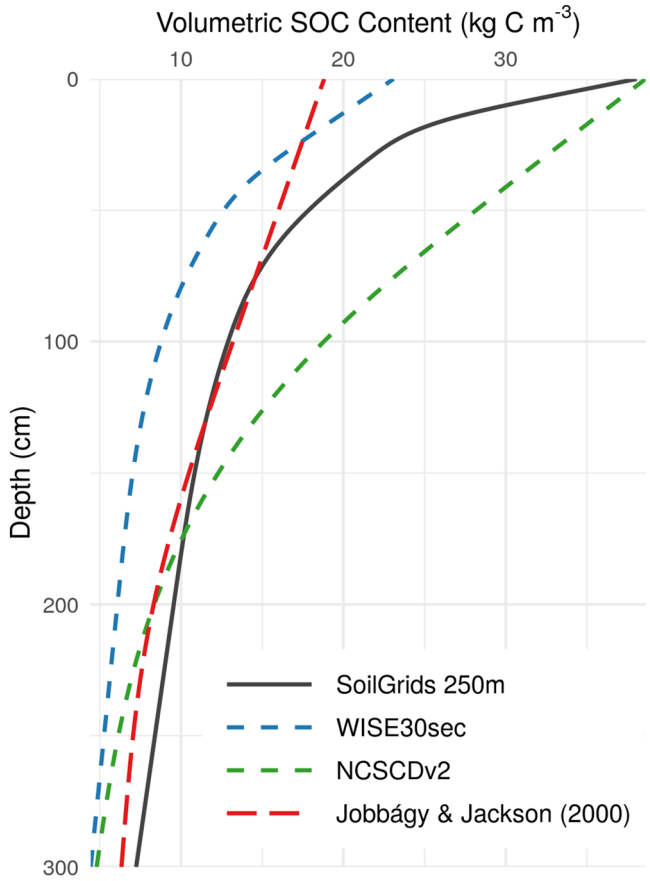

Figure 2. Depth profiles of SOC content derived from multiple global data sets and the Northern Circumpolar Soil Carbon Database, Version 2 (NCSCDv2), which is limited to the Circumpolar Arctic) shown as natural spline fits to the median SOC content in each layer.

also agree well, which is unsurprising given they are both based on the HWSD (FAO, 2009). We opted to use scaling ratios from SoilGrids for all subsequent comparisons to the L4C surface SOC data set, including 26.15% for 5- to 30-cm, 13.18% for 5- to 100-cm, and 7.83% for 5- to 300-cm areal SOC comparisons. However, for comparisons between the NCSCDv2 and L4C, the NCSCDv2 scaling ratio was used (13.04% for 5- to 300-cm).

The scaling factors derived from the depth profiles are consistent with prior estimates of global SOC stocks. Batjes (1996) (cited by Paustian et al., 2016) estimate of 684–724 Pg C in the top 30 cm is one of the earliest. Others cite a figure of 1,500 Pg C in the top 1 m of soil (Jobbágy & Jackson, 2000; Lal, 2004; Post et al., 2001), which is close to the average value found in a recent meta-analysis (Scharlemann et al., 2014), or approximately 2,300 Pg C in the top 3 m (Davidson & Janssens, 2006; Jobbágy & Jackson, 2000). Using the SoilGrids scaling factors to interpolate these different, deeper soil layer SOC estimates to that of the 0- to 5-cm layer, we obtain interpolated values in a narrow range from 182 to 195 Pg C.

3.2. Impact of SMAP Observations

The SMAP Tb observations had the greatest impact on L4C estimates of surface SOC and RH in regions where surface soil moisture levels are limiting (Figures 3a and 3b), namely, semiarid regions of the globe including Australia, southern Africa, the plains of North America, and the savanna highlands of Brazil. The impact of SMAP on surface SOC was relatively small (e.g., no more than 1.5% of total SOC, based on the normalized RMSD) compared with the large SOC stock size. However, the SMAP Tb observations had a much larger impact on RH (Figure 3b), accounting for as much 20% of this daily C flux. By analyzing the SMAP Tb impact along an aridity gradient (the precipitation-to-PET ratio), we found that the SMAP Tb observations had the greatest impact on the L4C carbon budget in semiarid regions where mean annual precipitation is less than mean annual PET, corresponding to about 59% of the global domain.

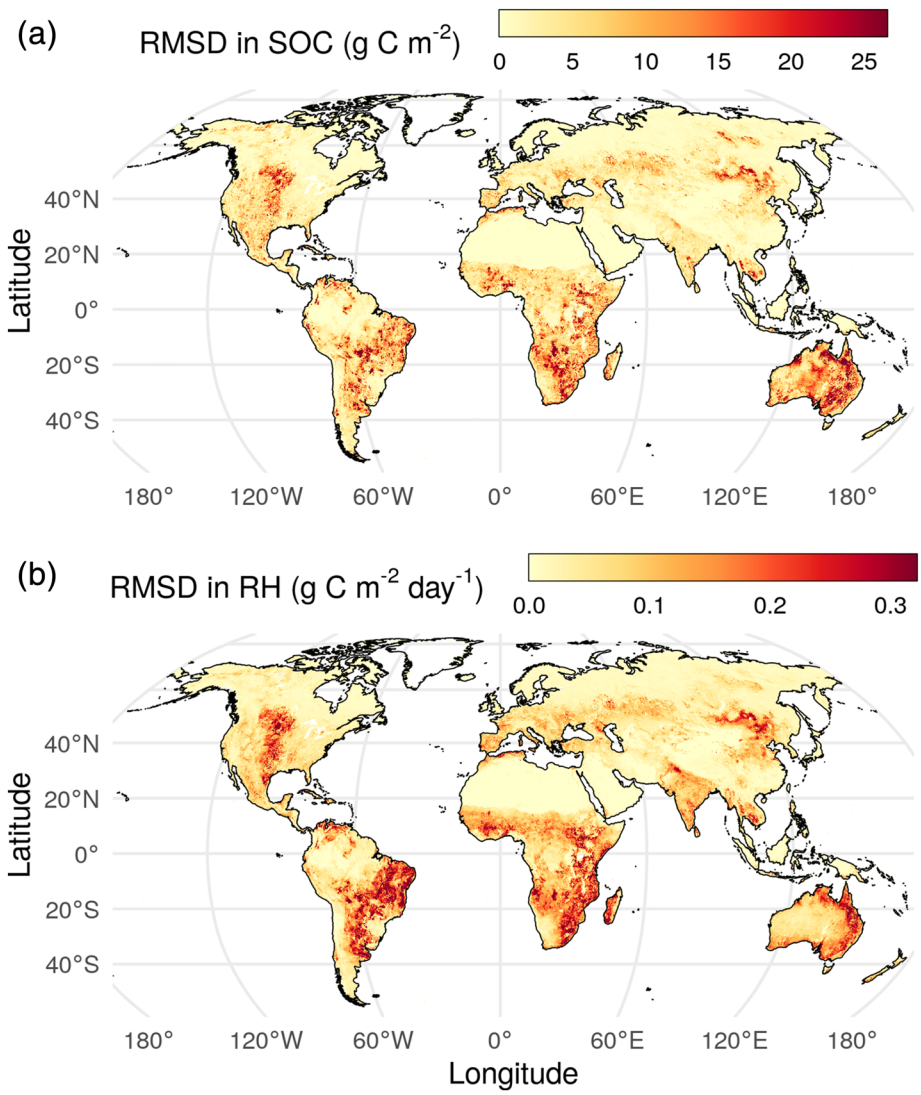

Figure 3. The impact of SMAP Tb observations on surface soil organic carbon (SOC) (a) and heterotrophic respiration (RH) (b) is quantified as the root-mean squared deviation (RMSD) between L4C Ops and Open Loop model runs, shown here for each pixel in the global modeling domain.

3.3. L4C SOC Compared to Alternative Assessments

The global distribution of L4C surface SOC seen in Figure 1 is generally consistent with other available global soil records across latitude bands (Figure 4), with correlation coefficients between latitude profiles ≥0.89. The L4C latitude profile shows favorable correspondence with both the TRENDYv7 ($r = 0.89$) and WISE30sec ($r = 0.97$) latitude profiles, which are based on an interpolation of surface SOC from deeper soil layers, and also with the SoilGrids (against L4C, $r = 0.96$) and GSED (against L4C, $r = 0.95$) profiles, which are not interpolated. However, the L4C product tends to show larger SOC stocks in the subtropics than the other records, particularly between 10° S and 40° S, which are areas dominated by shrub, grass, and cereal crop PFTs.

Compared to SoilGrids, the L4C profile shows higher SOC content throughout the temperate forests and semiarid regions of the world and especially in the subtropical grasslands of Africa and South America (Figure S6 in the supporting information). Conversely, the L4C product underestimates SOC relative to SoilGrids at high northern latitudes, particularly in shrublands, and in tropical evergreen broadleaf forests. A breakdown of SOC differences between L4C and the TRENDYv7 ensemble by PFT (Figure S8) indicates that, outside of the boreal region, the L4C SOC stocks are higher in cereal croplands, deciduous forests, and

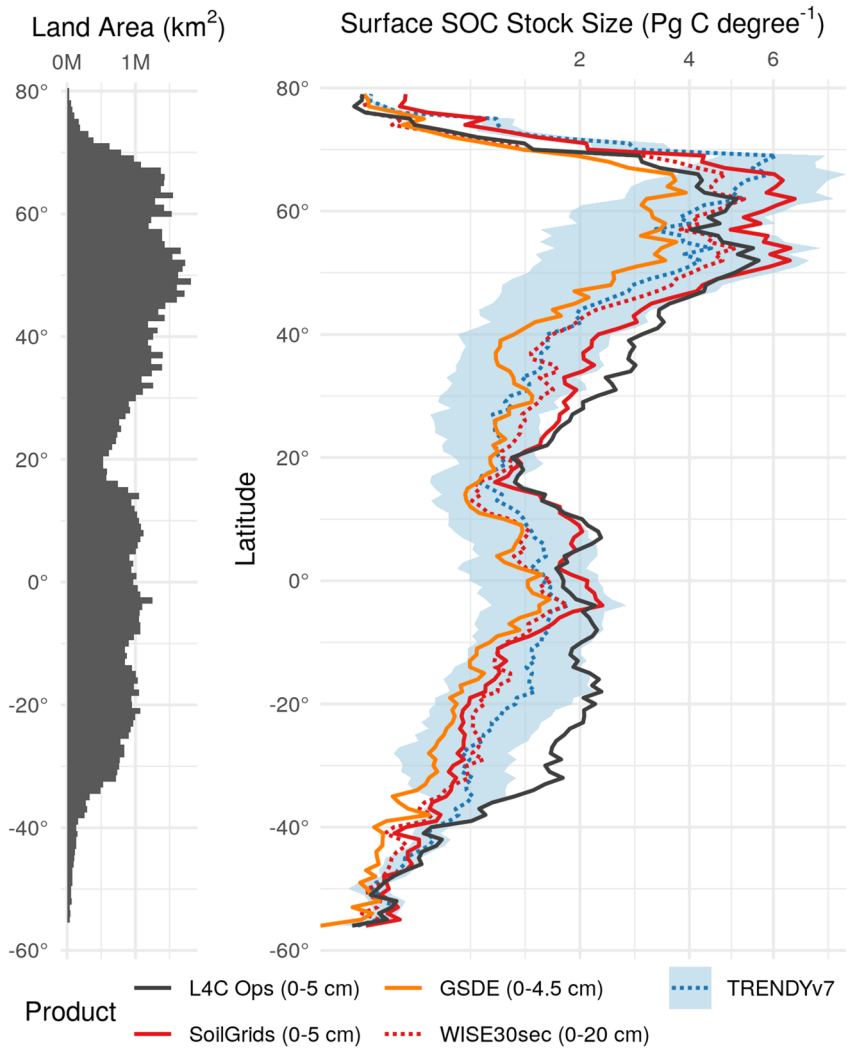

Figure 4. Global distribution of mean surface SOC estimates from multiple data sets, per degree of latitude (right) along with the L4C model land area per degree of latitude (left). Data sets shown with a dotted line are interpolated to a 5-cm surface soil layer consistent with the L4C SOC product. The TRENDYv7 ensemble mean is shown as a line; the shaded area corresponds to ±1 standard deviation in the associated model predictions.

grasslands. These PFTs, which generally have high litterfall residues, are the same as those where the L4C SOC stock is higher than in SoilGrids (Figure S9).

Two regional comparisons were also conducted: in the Circumpolar Arctic and in the contiguous United States (CONUS) plus Alaska. We compared L4C to the Circumpolar Arctic NCSCDv2 record by totaling L4C surface stocks within the irregular mapping units from that data set (Figure S2). The range of SOC pools thus represented compares very well in terms of total SOC stock size, after rescaling the NCSCDv2 values to represent surface (0–5 cm) SOC. Huntzinger et al. (2020) estimated benchmark SOC and total RH from observation data in the ABoVE domain for a model intercomparison; using Version 1 of the NCSCD, they estimated that the total SOC mass in the top 1 m of soil of the ABoVE Core domain, circa year 2000, is 84.59 Pg C, which is quite close to our estimate for the NCSCDv2 (82.65 Pg C). Using the SoilGrids scaling ratio to interpolate these 1-m estimates to 0–5 cm, we obtained 10.9–11.2 Pg C, which compared well with the 12.4 Pg C determined from the L4C SOC data set for the ABoVE Core domain in 2000. The Huntzinger et al. (2020) benchmark for total RH in this region, 1.43 Pg C year^{-1} (with a multimodel spread 0.41 to 2.13 Pg C year^{-1}), also compares well with the 1.14 Pg C year^{-1} estimate from the L4C RH data set in 2000.

In comparing the L4C and USDA FIA records for CONUS and Alaska, the overlapping period of record (2000–2007) was used. A comparison of the long-term mean state-wide totals in USDA FIA forest carbon

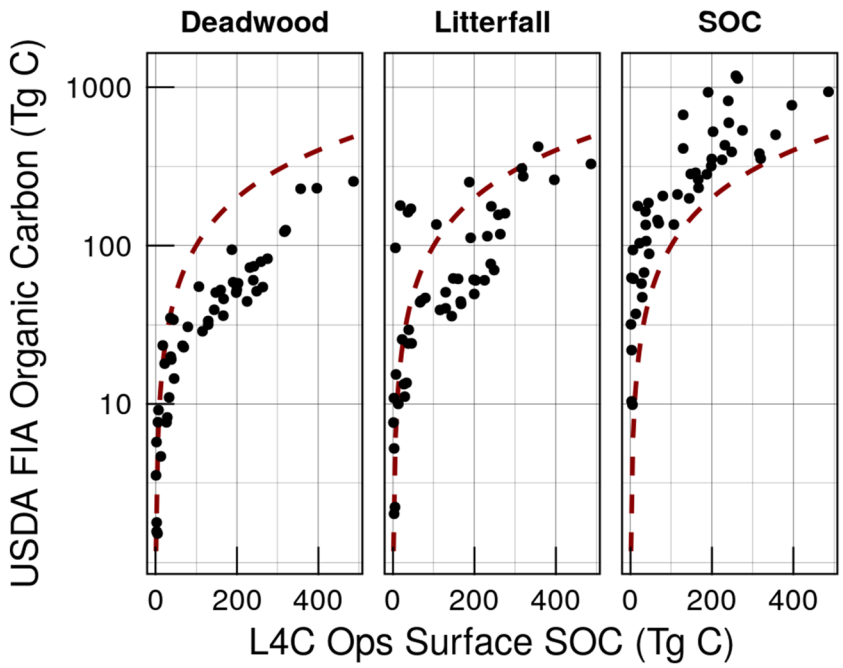

Figure 5. Log-linear plots of state-wide forest organic carbon totals. The long-term mean organic carbon stock from the U.S. Department of Agriculture (USDA) Forest Inventory and Analysis (FIA) data set in three different pools is plotted against the long-term mean forest soil organic carbon (SOC) from L4C. The 1:1 line is shown dashed in red.

and L4C surface SOC in forest lands is shown in Figure 5. The L4C surface SOC most closely corresponds to state litterfall totals in magnitude, with a correlation coefficient of $r = 0.73$ and a mean absolute difference (MAD) of 74 Tg C; L4C SOC also displays strong sublinear and superlinear correlations, respectively, to state totals in dead or downed wood ($r = 0.86$, MAD = 89 Tg C) and SOC ($r = 0.81$, MAD = 182 Tg C).

3.4. Surface SOC Stability

The global MRT distribution (Figure 6), based on L4C SOC, shows characteristically longer residence times at higher latitudes and altitudes, where soil decomposition is strongly constrained by cold temperatures: about 10–20 years longer than other regions. MRT values are intermediate over the temperate latitudes where soil decomposition is moderately constrained by seasonal soil moisture and temperature restrictions, whereas the MRT is shortest (0–1 years) in the wet tropics where soil moisture and temperature conditions are near optimum levels year-round for soil decomposition and RH. As the L4C surface SOC estimate represents topsoil conditions, the resulting MRT estimates are generally shorter than previous estimates for deeper soil stocks. A comparison of the annual RH flux in 2016 to a data-driven product linking climatic drivers with soil respiration observations (Tang et al., 2020) suggests that the L4C RH flux may be too high in those same areas where MRT is very low (Figure S7).

However, the spatial pattern of MRT is generally consistent with other maps and tabulations by biome (Carvalhais et al., 2014; Chen et al., 2013), where tundra, northern boreal forests, and montane grasslands and shrublands have the longest MRT estimates (Figure 6). Topsoil MRT values from L4C range from about 5–20 years for these biomes, whereas most other biomes have topsoil C turnover times of 4 years or less (Figure 7). We also compared the spatial distribution of L4C MRT to the 2011–2018 average temperature and precipitation estimates from CRU-TS4.03. We found a strong, exponential negative relationship between mean temperature and MRT (Spearman's $\rho = -0.76$) with a notable change point at the freezing point of water, above which the relationship is weak. As expected, the sensitivity of MRT to temperature is greater at higher latitudes (Chen et al., 2013), particularly at high northern latitudes (Figure S10). MRT also declines with mean annual precipitation ($\rho = -0.80$).

3.5. Surface SOC Dynamics

The seasonal dynamics of L4C SOC, NPP, and RH vary by region (Figure 8), but, in general, the slower evolution of surface SOC lags the more dynamic changes in NPP and RH by up to several months. The surface

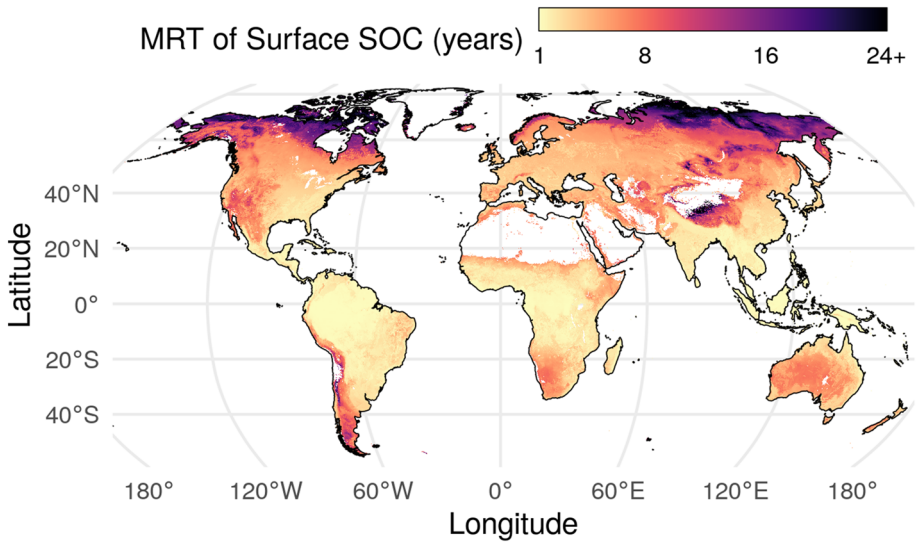

Figure 6. Map of average mean residence time (MRT), in years, from the L4C heterotophic respiration (RH) and surface soil organic carbon (SOC) products. Areas in white represent barren, sparsely vegetated, or open water areas outside of the product domain.

SOC response is buffered by the cascading L4C soil C pools of varying sizes and decomposition rates, which together influence the bulk RH rate (Jones et al., 2017). The seasonal cycle and any potential interannual secular variation dominates the temporal variation in surface SOC, while the remaining, unexplained variation represented by the detrended anomalies (Equation 2) accounts for only 3% of the global surface SOC temporal variance. However, the detrended anomalies account for as much as 17% of the temporal variation in SOC in much of the Southern Hemisphere and over 50% of the variation in some parts of the world. In

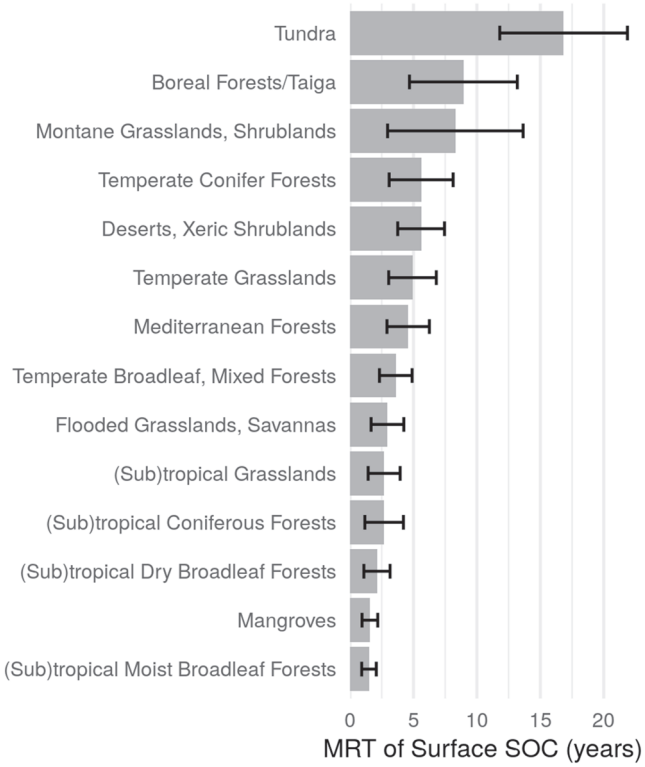

Figure 7. Average mean residence time (MRT) of L4C surface soil organic carbon (SOC), summarized within terrestrial ecoregions. Error bars denote one spatial standard deviation.

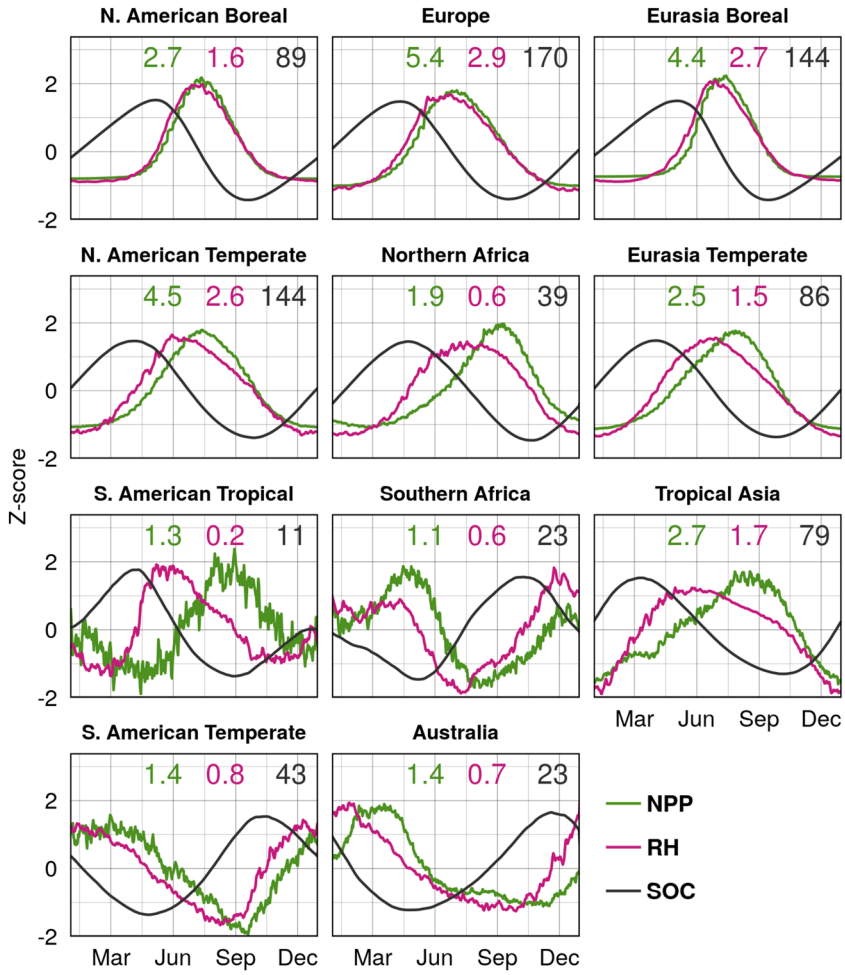

Figure 8. Seasonal dynamics of surface soil organic carbon (SOC), net primary productivity (NPP), and heterotrophic respiration (RH) by TransCom region. *Z* scores are calculated for each day of the year based on the 20-year harmonized L4C Ops and Nature Run time series, following bias correction of the Nature Run values. *Z* scores remove important differences in magnitudes between each region, so the seasonal amplitudes (maximum minus minimum value) for SOC ($g\,C\,m^{-2}$), NPP ($g\,C\,m^{-2}\,day^{-1}$), and RH ($g\,C\,m^{-2}\,day^{-1}$) are also reported at the top-right of each plot.

carbon terms, seasonal amplitudes in surface SOC may be as high as 200 $g\,C\,m^{-2}$, and daily anomalies may account for 1 $g\,C\,m^{-2}$ or more (Figure S3).

The sensitivity analysis (Equation 4) shows that the ΔSOC anomalies are much more sensitive to changes in RH than NPP (not shown). The ΔSOC anomalies have a strong negative sensitivity to RH anomalies, as expected, throughout the globe; however, this sensitivity is generally strongest in the driest (e.g., tundra and deserts) and wettest (e.g., tropical rain forest) biomes. The ΔSOC and RH anomaly time series are anti-correlated at $|r| \geq 0.85$ across all TransCom regions. Conversely, the ΔSOC sensitivity to NPP anomalies is relatively weak (median RH p value $\ll 0.001$, median NPP p value $= 0.058$ for zero monthly lag), whereby much of the globe showed an expected positive sensitivity to NPP anomalies while other areas showed no apparent sensitivity. Broadleaf croplands, deciduous forests, and grasslands were the only PFTs to display a significant ΔSOC sensitivity to NPP, with deciduous needleleaf forests having the highest sensitivity. The ΔSOC and NPP anomaly time series show regional correlations ranging from $r = 0.10$ in Tropical Asia to $r = 0.77$ in the North American Boreal region, whereas the regional correlations between ΔSOC and RH anomalies range from $r = 0.85$ to $r = 0.98$.

When ΔSOC anomalies lagged NPP and RH anomalies by 1 month, sensitivity to RH declined considerably, but sensitivity to NPP was about the same. When we examined sensitivity to NPP or RH changes two or

more months prior to change in SOC, RH has no effect (80th percentile p value = 0.160), but sensitivity to NPP persisted for some regions (80th percentile p value = 0.007) up to 3 months prior.

While RH and NPP from the TRENDYv7 models are available on a monthly basis, the associated model SOC data are only available on an annual basis, so a similar sensitivity analysis was not conducted. However, a comparison of the detrended anomaly time series for L4C and TRENDYv7 shows good concordance in RH dynamics in most regions and in NPP dynamics outside of the tropics (Figures S4 and S5). The L4C and TRENDYv7 ensemble mean monthly correlations for RH were highest in the North American Boreal ($r = 0.70$), North American Temperate ($r = 0.69$), and Northern Africa ($r = 0.61$) regions. The model NPP correlations were generally higher than for RH and highest in the same regions but also in the Eurasia Temperate ($r = 0.79$), Europe ($r = 0.69$), and Australia ($r = 0.83$) regions; these results indicate that the model NPP dynamics are in good agreement at high latitudes and in the boreal and temperate regions.

4. Discussion

The SMAP L4C global SOC distribution was generally consistent with other available assessments from soil inventories and the TRENDYv7 model simulations. Regional differences in SOC stock size between L4C and other SOC products may reflect one or more factors, including an uneven global distribution of soil inventory sites, model error contributed from climate drivers, and land management uncertainty. In particular, L4C estimates indicate higher SOC storage in the subtropics (20–40° north or south) than previous estimates, and it is possible that the true distribution of global SOC may have been previously underestimated in this and other regions. Tifafi et al. (2018) reported that global inventories tend to underestimate SOC relative to field data and that SoilGrids presents a slight improvement over prior estimates that were biased too low. The L4C results revise this estimate higher by about 1 Pg C per degree of latitude in the subtropics compared to alternative assessments (Figure 4). Zhao et al. (2019) also recently estimated higher global SOC storage in the 0- to 30-cm soil layer relative to the Batjes (1996) popularly cited estimate.

The L4C results indicate that surface SOC is a dynamic quantity, with seasonal amplitudes over 100 g C m^{-2} in temperate North America, Europe, and the Eurasia Boreal region (Figure S3). Changes beyond the expected seasonal variation account for more than 0.4 g C m^{-2} day^{-1} in temperate North America. The influence of the SMAP L-band soil moisture observations on the L4C SOC estimates was relatively minor (~1.5%) outside of semiarid regions and was particularly weak in the high northern boreal and tundra regions (Figure 3). However, the impact accounted for as much as 20% of the estimated daily RH flux in much of Africa, South America, and Australia. The SMAP influence on the L4C SOC estimates was greatest in semiarid regions, encompassing almost 60% of the global domain. In these dryland regions, the carbon budget is strongly constrained by available moisture, and the SMAP L-band soil signal is enhanced by the characteristic low-to-moderate vegetation cover (Jones et al., 2017).

The influence of SMAP is also expected to be greater in regions where in situ precipitation measurement networks are sparse; these network observations are assimilated, along with SMAP Tb retrievals and other observations, into the GEOS-5 Catchment Land Model for the L4SM production (Reichle et al., 2017). Thus, the relative influence of SMAP on the L4SM (and L4C) predictions is less where the land model-assimilated precipitation information is more robust. As a result, the global impact of SMAP on the L4C predictions (Figure 3) is smaller than the influence of soil moisture and temperature on the carbon model predictions (Jones et al., 2017).

Dynamic changes in L4C SOC, represented by C losses due to RH and C inputs from NPP, correspond well with more sophisticated DGVM C-flux simulations represented by the TRENDYv7 ensemble, which use different forcing data and explicitly account for the influence of increasing atmospheric CO_2 levels. The L4C model may partially account for the influence of atmospheric CO_2 trends through the associated response in MODIS observed photosynthetic vegetation cover (fPAR) used as a model input for estimating NPP. In L4C, the primary driver of seasonally adjusted, monthly SOC dynamics is RH, while the influence of NPP is much smaller, with a longer lagged effect. This behavior manifests from the litterfall C allocation to multiple interconnected soil pools, including those with very slow turnover times; the NPP contribution is also closely tied to the seasonal cycle. The L4C behavior is consistent with previous studies indicating a strong climate control on NPP and litterfall (Chu et al., 2016; Del Grosso et al., 2008) but a weaker direct relationship between productivity and SOC density (Zhao et al., 2019). Tifafi et al. (2018) also found that climatic variation principally affected soil carbon outputs (i.e., respiration) rather than inputs.

Unlike many other SOC products that represent deeper soil profiles, the L4C product represents topsoil conditions within the 0- to 5-cm layer. While this surface storage only represents 5–13% of the total soil profile SOC stock (Figure 2), it is relatively labile, with the highest biological activity (Schindlbacher et al., 2010) and the greatest contribution toward soil RH flux (Bond-Lamberty et al., 2004). The L4C SOC has an expected shorter (5–20 year) MRT than other SOC assessments representing deeper soil layers (Chen et al., 2013) or more comprehensive carbon budgets (Carvalhais et al., 2014). We explicitly recognized the varying soil layer depths used in different soil data records and investigated soil carbon depth profiles (Figure 2) to interpolate SOC estimates to a standard surface layer (0–5 cm). As a result, we found generally good agreement between the different SOC products in latitudinal distributions and in global and regional stock estimates relative to prior assessments (e.g., Huntzinger et al., 2020), which have reported considerable divergence in global or regional estimates of SOC distribution and storage (Gray & Bishop, 2016; Tifafi et al., 2018; Todd-Brown et al., 2013) and trends (Wieder et al., 2018).

The apparent SOC uncertainty is greatest in the surface soil layer (Figure 2), where the L4C product may contribute to better understanding. The diversity of estimates available suggests that the processes determining SOC protection and degradation are not well understood at landscape to global scales (O'Rourke et al., 2015). However, it is more productive to view the diversity of inventories and models as an ensemble that spans a significant range of the process uncertainty in SOC estimates (e.g., Carvalhais et al., 2014; Tian et al., 2015; Wieder et al., 2018). Just as the ensemble mean in climate models and DGVMs is generally accepted as more reliable than any individual estimate, the multiple approaches to estimating global SOC complement one another as we learn more about the processes that constrain SOC decomposition or protection across scales (Crowther et al., 2019).

There are two distinct L4C limitations that may be addressed in future product versions. First, land use and land cover change, particularly those due to human disturbances, are not explicitly represented, nor are land management practices. These activities can have significant regional impacts on SOC (Harden et al., 2018; Luo et al., 2017), in addition to climate variability, but are challenging to capture in global assessments. Second, there are some mechanisms recently recognized as important for SOC dynamics that have yet to be formally represented in global earth system and terrestrial carbon models like L4C (Luo et al., 2016). The role of microbial biomass in the stabilization and transformation of SOC is the most conspicuous missing piece of these models (Wieder et al., 2013), and, despite increasing global data availability (Crowther et al., 2019), it is perhaps the most difficult to parameterize for operational, global models. The emerging view of SOC dynamics emphasizes not just microbial functions but also substrate availability (Lehmann & Kleber, 2015; Luo et al., 2017) and the dynamic protection of mineral SOC that is partially dependent on soil texture and composition (Cagnarini et al., 2019). The quality and type of litter inputs as a function of the vegetation community is another missing piece (Hu et al., 2018) that affects the microbial influence on SOC dynamics but may be parameterized more easily than microbial functions in future models.

5. Conclusions

The SMAP L4C product provides a daily global carbon budget that includes surface SOC dynamics sensitive to short-term climate variability. The satellite data-driven L4C algorithm combines MODIS vegetation observations with SMAP soil moisture and temperature as key drivers for estimating SOC and component carbon fluxes. The L4C outputs are mapped to a consistent 9-km global grid that preserves subgrid (1-km) scale information for up to eight individual PFT classes; this multiscale product structure facilitates both global applications at the level of earth system model projections and finer landscape delineations required for many environmental applications.

The L4C SOC parameter represents the surface (0- to 5-cm depth) soil layer carbon stock at the interface between a dynamic lower atmosphere and more stable SOC in deeper soil layers. SMAP measurements of temperature and moisture in this surface layer enhance L4C capabilities for estimating labile SOC, which is crucial for soil health because productivity inputs to this layer quantify the amount of carbon available for mineralization. The relative impact of SMAP observations on L4C SOC is also greater in global dryland regions, which are a major driver of interannual variability in the terrestrial carbon sink (Ahlström et al., 2015; Poulter et al., 2014). Despite the wide disagreement in SOC stock distributions among global models and inventories, when differences in modeled soil depths are taken into account, the L4C SOC product agrees well with other global and regional estimates of surface SOC. L4C is an operational product of

the NASA SMAP mission incorporates ongoing sensor and model calibration and validation refinements. The L4C data set extends from 2015 to the present with continuing, daily observations available approximately every 10 days. These observations provide new capacity for the global monitoring of soil health, while enabling prognostic investigations into the effects of relatively transient climatic events (e.g., droughts and pluvials) on SOC and the terrestrial carbon balance.

Data Availability Statement

The SMAP L4C operational product (Version 4) is publicly accessible through the National Snow and Ice Data Center (NSIDC) (at https://nsidc.org/data/SPL4CMDL/versions/4). The SMAP L4C Nature Run (v7.2) is available through a public FTP site (see http://doi.org/10.5281/zenodo.4247969). Derived data used in this study and the software required to reproduce results are available online (at http://doi.org/10.5281/zenodo.4266454).

Acknowledgments
This study was supported with funding from NASA (NNX14AI50G, NNX16AN05G, 80NSSC17K0115, 80NSSC18K0980, and NNH17ZDA001N-NIP).

References

Ahlström, A., Raupach, M. R., Schurgers, G., Smith, B., Arneth, A., Jung, M., et al. (2015). The dominant role of semi-arid ecosystems in the trend and variability of the land CO_2 sink. *Science*, *348*(6237), 895–899. https://doi.org/10.1126/science.aaa1668

Bünemann, E. K., Bongiorno, G., Bai, Z., Creamer, R. E., De Deyn, G., de Goede, R., et al. (2018). Soil quality: A critical review. *Soil Biology and Biochemistry*, *120*, 105–125. https://doi.org/10.1016/j.soilbio.2018.01.030

Baker, D. F., Law, R. M., Gurney, K. R., Rayner, P., Peylin, P., Denning, A. S., et al. (2006). TransCom 3 inversion intercomparison: Impact of transport model errors on the interannual variability of regional CO_2 fluxes, 1988–2003. *Global Biogeochemical Cycles*, *20*, GB1002. https://doi.org/10.1029/2004GB002439

Baldocchi, D. (2008). "Breathing" of the terrestrial biosphere: Lessons learned from a global network of carbon dioxide flux measurement systems. *Australian Journal of Botany*, *56*(1), 1. https://doi.org/10.1071/BT07151

Batjes, N. H. (1996). Total carbon and nitrogen in the soils of the world. *European Journal of Soil Science*, *65*(1), 10–21. https://doi.org/10.1111/ejss.12114_2

Batjes, N. H. (2016). Harmonized soil property values for broad-scale modelling (WISE30sec) with estimates of global soil carbon stocks. *Geoderma*, *269*, 61–68. https://doi.org/10.1016/j.geoderma.2016.01.034

Bloom, A. A., Exbrayat, J.-F., van der Velde, I. R., Feng, L., & Williams, M. (2016). The decadal state of the terrestrial carbon cycle: Global retrievals of terrestrial carbon allocation, pools, and residence times. *Proceedings of the National Academy of Sciences*, *113*(5), 1285–1290. https://doi.org/10.1073/pnas.1515160113

Bond-Lamberty, B., Bailey, V. L., Chen, M., Gough, C. M., & Vargas, R. (2018). Globally rising soil heterotrophic respiration over recent decades. *Nature*, *560*(7716), 80–83. https://doi.org/10.1038/s41586-018-0358-x

Bond-Lamberty, B., Wang, C., & Gower, S. T. (2004). A global relationship between the heterotrophic and autotrophic components of soil respiration? *Global Change Biology*, *10*(10), 1756–1766. https://doi.org/10.1111/j.1365-2486.2004.00816.x

Borken, W., Savage, K., Davidson, E. A., & Trumbore, S. E. (2006). Effects of experimental drought on soil respiration and radiocarbon efflux from a temperate forest soil. *Global Change Biology*, *12*(2), 177–193. https://doi.org/10.1111/j.1365-2486.2005.001058.x

Bradford, M. A., Wieder, W. R., Bonan, G. B., Fierer, N., Raymond, P. A., & Crowther, T. W. (2016). Managing uncertainty in soil carbon feedbacks to climate change. *Nature Climate Change*, *6*(8), 751–758. https://doi.org/10.1038/nclimate3071

Brodzik, M. J., Billingsley, B., Haran, T., Raup, B., & Savoie, M. H. (2012). EASE-Grid 2.0: Incremental but significant improvements for Earth-gridded data sets. *ISPRS International Journal of Geo-Information*, *1*(3), 32–45. https://doi.org/10.3390/ijgi1010032

Burke, M., & Lobell, D. B. (2017). Satellite-based assessment of yield variation and its determinants in smallholder African systems. *Proceedings of the National Academy of Sciences*, *114*(9), 2189–2194. https://doi.org/10.1073/pnas.1616919114

Cagnarini, C., Blyth, E., Emmett, B. A., Evans, C. D., Griffiths, R. I., Keith, A., et al. (2019). Zones of influence for soil organic matter dynamics: A conceptual framework for data and models. *Global Change Biology*, *25*(12), 3996–4007. https://doi.org/10.1111/gcb.14787

Carvalhais, N., Forkel, M., Khomik, M., Bellarby, J., Jung, M., Migliavacca, M., et al. (2014). Global covariation of carbon turnover times with climate in terrestrial ecosystems. *Nature*, *514*(7521), 213–217. https://doi.org/10.1038/nature13731

Chen, S., Huang, Y., Zou, J., & Shi, Y. (2013). Mean residence time of global topsoil organic carbon depends on temperature, precipitation and soil nitrogen. *Global and Planetary Change*, *100*, 99–108. https://doi.org/10.1016/j.gloplacha.2012.10.006

Chu, C., Bartlett, M., Wang, Y., He, F., Weiner, J., Chave, J., & Sack, L. (2016). Does climate directly influence NPP globally? *Global Change Biology*, *22*(1), 12–24. https://doi.org/10.1111/gcb.13079

Conant, R. T., Dalla-Betta, P., Klopatek, C. C., & Klopatek, J. M. (2004). Controls on soil respiration in semiarid soils. *Soil Biology and Biochemistry*, *36*(6), 945–951. https://doi.org/10.1016/j.soilbio.2004.02.013

Crowther, T. W., Todd-Brown, K. E. O., Rowe, C. W., Wieder, W. R., Carey, J. C., MacHmuller, M. B., et al. (2016). Quantifying global soil carbon losses in response to warming. *Nature*, *540*(7631), 104–108. https://doi.org/10.1038/nature20150

Crowther, T. W., van den Hoogen, J., Wan, J., Mayes, M. A., Keiser, A. D., Mo, L., et al. (2019). The global soil community and its influence on biogeochemistry. *Science*, *365*(6455). https://doi.org/10.1126/science.aav0550

Davidson, E. A., & Janssens, I. A. (2006). Temperature sensitivity of soil carbon decomposition and feedbacks to climate change. *Nature*, *440*(7081), 165–173. https://doi.org/10.1038/nature04514

Del Grosso, S., Parton, W., Stohlgren, T., Zheng, D., Bachelet, D., Prince, S., et al. (2008). Global potential net primary production predicted from vegetation class, precipitation, and temperature. *Ecology*, *89*(8), 2117–2126. https://doi.org/10.1890/07-0850.1

Dietzen, C. A., Larsen, K. S., Ambus, P. L., Michelsen, A., Arndal, M. F., Beier, C., et al. (2019). Accumulation of soil carbon under elevated CO_2 unaffected by warming and drought. *Global Change Biology*, *2*(January), 2970–2977. https://doi.org/10.1111/gcb.14699

Endsley, K. A., Jones, L. A., & Kimball, J. S. (2020). Soil Moisture Active/Passive (SMAP) Level 4 Carbon (L4C) Nature Run Version 7.2. https://doi.org/10.5281/zenodo.4247969

Entekhabi, D., Reichle, R. H., Koster, R. D., & Crow, W. T. (2010). Performance metrics for soil moisture retrievals and application requirements. *Journal of Hydrometeorology*, *11*(3), 832–840. https://doi.org/10.1175/2010JHM1223.1

Euskirchen, E. S., Mcguire, A. D., Kicklighter, D. W., Zhuang, Q., Clein, J. S., Dargaville, R. J., et al. (2006). Importance of recent shifts in soil thermal dynamics on growing season length, productivity, and carbon sequestration in terrestrial high-latitude ecosystems. *Global Change Biology*, *12*(4), 731–750. https://doi.org/10.1111/j.1365-2486.2006.01113.x

FAO (2009). Harmonized World Soil Database, Version 1.1. Rome and Laxenberg: Food and Agriculture Organization of the United Nations.

Friedl, M. A., Sulla-Menashe, D., Tan, B., Schneider, A., Ramankutty, N., Sibley, A., & Huang, X. (2010). MODIS Collection 5 global land cover: Algorithm refinements and characterization of new datasets. *Remote Sensing of Environment*, *114*(1), 168–182. https://doi.org/10.1016/j.rse.2009.08.016

Gelaro, R., McCarty, W., Suárez, M. J., Todling, R., Molod, A., Takacs, L., et al. (2017). The Modern-Era Retrospective Analysis for Research and Applications, Version 2 (MERRA-2). *Journal of Climate*, *30*(14), 5419–5454. https://doi.org/10.1175/JCLI-D-16-0758.1

Gray, J. M., & Bishop, T. F. A. (2016). Change in soil organic carbon stocks under 12 climate change projections over New South Wales, Australia. *Soil Science Society of America Journal*, *80*(5), 1296–1307. https://doi.org/10.2136/sssaj2016.02.0038

Harden, J. W., Hugelius, G., Ahlström, A., Blankinship, J. C., Bond-Lamberty, B., Lawrence, C. R., et al. (2018). Networking our science to characterize the state, vulnerabilities, and management opportunities of soil organic matter. *Global Change Biology*, *24*(2), e705–e718. https://doi.org/10.1111/gcb.13896

Harris, I., Jones, P. D., Osborn, T. J., & Lister, D. H. (2014). Updated high-resolution grids of monthly climatic observations—The CRU TS3.10 dataset. *International Journal of Climatology*, *34*(3), 623–642. https://doi.org/10.1002/joc.3711

Hengl, T., De Jesus, J. M., Heuvelink, G. B. M., Gonzalez, M. R., Kilibarda, M., Blagotić, A., et al. (2017). SoilGrids250m: Global gridded soil information based on machine learning. *PLoS ONE*, *12*(2), 1–40. https://doi.org/10.1371/journal.pone.0169748

Hicks Pries, C. E., Castanha, C., Porras, R. C., & Torn, M. S. (2017). The whole-soil carbon flux in response to warming. *Science*, *355*(6332), 1420–1423. https://doi.org/10.1126/science.aal1319

Hobley, E., Wilson, B., Wilkie, A., Gray, J., & Koen, T. (2015). Drivers of soil organic carbon storage and vertical distribution in Eastern Australia. *Plant and Soil*, *390*(1–2), 111–127. https://doi.org/10.1007/s11104-015-2380-1

Hu, Z., Michaletz, S. T., Johnson, D. J., McDowell, N. G., Huang, Z., Zhou, X., & Xu, C. (2018). Traits drive global wood decomposition rates more than climate. *Global Change Biology*, *24*(11), 5259–5269. https://doi.org/10.1111/gcb.14357

Hugelius, G., Strauss, J., Zubrzycki, S., Harden, J. W., Schuur, E. A. G., Ping, C. L., et al. (2014). Estimated stocks of circumpolar permafrost carbon with quantified uncertainty ranges and identified data gaps. *Biogeosciences*, *11*(23), 6573–6593. https://doi.org/10.5194/bg-11-6573-2014

Hugelius, G., Tarnocai, C., Broll, G., Canadell, J. G., Kuhry, P., & Swanson, D. K. (2013). The Northern Circumpolar Soil Carbon Database: Spatially distributed datasets of soil coverage and soil carbon storage in the northern permafrost regions. *Earth System Science Data*, *5*(1), 3–13. https://doi.org/10.5194/essd-5-3-2013

Huntzinger, D. N., Schaefer, K., Schwalm, C., Fisher, J. B., Hayes, D., Stofferahn, E., et al. (2020). Evaluation of simulated soil carbon dynamics in Arctic-Boreal ecosystems. *Environmental Research Letters*, *15*(2), 025005. https://doi.org/10.1088/1748-9326/ab6784

Hursh, A., Ballantyne, A. P., Cooper, L., Maneta, M., Kimball, J., & Watts, J. (2017). The sensitivity of soil respiration to soil temperature, moisture, and carbon supply at the global scale. *Global Change Biology*, *23*(5), 2090–2103. https://doi.org/10.1111/gcb.13489

Jobbágy, E. G., & Jackson, R. B. (2000). The vertical distribution of soil organic carbon and its relation to climate and vegetation. *Ecological Applications*, *10*(2), 423–436. https://doi.org/10.1890/1051-0761(2000)010[0423:TVDOSO]2.0.CO;2

Jones, L. A., Kimball, J. S., Reichle, R. H., Madani, N., Glassy, J., Ardizzone, J. V., et al. (2017). The SMAP Level 4 Carbon product for monitoring ecosystem land-atmosphere CO_2 exchange. *IEEE Transactions on Geoscience and Remote Sensing*, *55*(11), 6517–6532. https://doi.org/10.1109/TGRS.2017.2729343

Jung, M., Reichstein, M., Schwalm, C. R., Huntingford, C., Sitch, S., Ahlström, A., et al. (2017). Compensatory water effects link yearly global land CO_2 sink changes to temperature. *Nature*, *541*(7638), 516–520. https://doi.org/10.1038/nature20780

Köchy, M., Hiederer, R., & Freibauer, A. (2015). Global distribution of soil organic carbon Part 1: Masses and frequency distributions of SOC stocks for the tropics, permafrost regions, wetlands, and the world. *SOIL*, *1*(1), 351–365. https://doi.org/10.5194/soil-1-351-2015

Kim, Y., Kimball, J. S., Zhang, K., & McDonald, K. C. (2012). Satellite detection of increasing Northern Hemisphere non-frozen seasons from 1979 to 2008: Implications for regional vegetation growth. *Remote Sensing of Environment*, *121*, 472–487. https://doi.org/10.1016/j.rse.2012.02.014

Kwon, M. J., Natali, S. M., Hicks Pries, C. E., Schuur, E. A. G., Steinhof, A., Crummer, K. G., et al. (2019). Drainage enhances modern soil carbon contribution but reduces old soil carbon contribution to ecosystem respiration in tundra ecosystems. *Global Change Biology*, *25*(4), 1315–1325. https://doi.org/10.1111/gcb.14578

Lal, R. (2004). Soil carbon sequestration impacts on global climate change and food security. *Science*, *304*(5677), 1623–1627. https://doi.org/10.1126/science.1097396

Le Quéré, C., Barbero, L., Hauck, J., Andrew, R. M., Canadell, J. G., Sitch, S., & Korsbakken, J. I. (2018). Global Carbon Budget 2018. *Earth System Science Data*, *10*(April 2017), 2141–2194.

Lehmann, J., & Kleber, M. (2015). The contentious nature of soil organic matter. *Nature*, *528*(7580), 60–68. https://doi.org/10.1038/nature16069

Lucchesi, R. (2018). File specification for GEOS FP. GMAO Office Note No. 4 (Version1.2). Greenbelt, Maryland, U.S.A.: Global Modeling and Assimilation Office, Earth Sciences Division, NASA Goddard Space Flight Center.

Luo, Y., Ahlström, A., Allison, S. D., Batjes, N. H., Brovkin, V., Carvalhais, N., et al. (2016). Toward more realistic projections of soil carbon dynamics by Earth system models. *Global Biogeochemical Cycles*, *30*, 40–56. https://doi.org/10.1002/2015GB005239

Luo, Z., Baldock, J., & Wang, E. (2017). Modelling the dynamic physical protection of soil organic carbon: Insights into carbon predictions and explanation of the priming effect. *Global Change Biology*, *23*(12), 5273–5283. https://doi.org/10.1111/gcb.13793

Luo, Z., Feng, W., Luo, Y., Baldock, J., & Wang, E. (2017). Soil organic carbon dynamics jointly controlled by climate, carbon inputs, soil properties and soil carbon fractions. *Global Change Biology*, *23*(10), 4430–4439. https://doi.org/10.1111/gcb.13767

O'Rourke, S. M., Angers, D. A., Holden, N. M., & Mcbratney, A. B. (2015). Soil organic carbon across scales. *Global Change Biology*, *21*(10), 3561–3574. https://doi.org/10.1111/gcb.12959

Olson, D. M., Dinerstein, E., Wikramanayake, E. D., Burgess, N. D., Powell, G. V. N., Underwood, E. C., et al. (2001). Terrestrial ecoregions of the world: A new map of life on Earth. *BioScience*, *51*(11), 933. https://doi.org/10.1641/0006-3568(2001)051[0933:TEOTWA]2.0.CO;2

Park, T., Ganguly, S., Tømmervik, H., Euskirchen, E. S., Høgda, K.-A., Karlsen, S. R., et al. (2016). Changes in growing season duration and productivity of northern vegetation inferred from long-term remote sensing data. *Environmental Research Letters*, *11*(8), 084001. https://doi.org/10.1088/1748-9326/11/8/084001

Paustian, K., Lehmann, J., Ogle, S., Reay, D., Robertson, G. P., & Smith, P. (2016). Climate-smart soils. *Nature*, *532*(7597), 49–57. https://doi.org/10.1038/nature17174

Post, W. M., Izaurralde, R. C., Mann, L. K., & Bliss, N. (2001). Monitoring and verifying changes of organic carbon in soil. *Climatic Change*, *51*(1), 73–99. https://doi.org/10.1023/A:1017514802028

Poulter, B., Frank, D., Ciais, P., Myneni, R. B., Andela, N., Bi, J., et al. (2014). Contribution of semi-arid ecosystems to interannual variability of the global carbon cycle. *Nature*, *509*(7502), 600–603. https://doi.org/10.1038/nature13376

Pugnaire, F. I., Morillo, J. A., Peñuelas, J., Reich, P. B., Bardgett, R. D., Gaxiola, A., et al. (2019). Climate change effects on plant-soil feedbacks and consequences for biodiversity and functioning of terrestrial ecosystems. *Science Advances*, *5*(11), 1–12. https://doi.org/10.1126/sciadv.aaz1834

Reichle, R. H., De Lannoy, G., Koster, R. D., Crow, W. T., Kimball, J. S., & Liu, Q. (2019). SMAP L4 Global 3-hourly 9 km EASE-Grid Surface and Root Zone Soil Moisture Geophysical Data, Version 4, Boulder, Colorado, U.S.A. https://doi.org/10.5067/KPJNN2GI1DQR

Reichle, R. H., De Lannoy, G. J. M., Liu, Q., Ardizzone, J. V., Colliander, A., Conaty, A., et al. (2017). Assessment of the SMAP Level-4 surface and root-zone soil moisture product using in situ measurements. *Journal of Hydrometeorology*, *18*(10), 2621–2645. https://doi.org/10.1175/JHM-D-17-0063.1

Reichle, R. H., De Lannoy, G. J. M., Liu, Q., Koster, R. D., Kimball, J. S., Crow, W. T., et al. (2017). Global assessment of the SMAP Level-4 surface and root-zone soil moisture product using assimilation diagnostics. *Journal of Hydrometeorology*, *18*(12), 3217–3237. https://doi.org/10.1175/JHM-D-17-0130.1

Reichle, R. H., Liu, Q., Koster, R. D., Crow, W. T., De Lannoy, G. J. M., Kimball, J. S., et al. (2019). Version 4 of the SMAP Level 4 soil moisture algorithm and data product. *Journal of Advances in Modeling Earth Systems*, *11*(10), 3106–3130. https://doi.org/10.1029/2019MS001729

Scharlemann, J. P. W., Tanner, E. V. J., Hiederer, R., & Kapos, V. (2014). Global soil carbon: Understanding and managing the largest terrestrial carbon pool. *Carbon Management*, *5*(1), 81–91. https://doi.org/10.4155/cmt.13.77

Schindlbacher, A., de Gonzalo, C., Díaz-Pinés, E., Gorría, P., Matthews, B., Inclán, R., et al. (2010). Temperature sensitivity of forest soil organic matter decomposition along two elevation gradients. *Journal of Geophysical Research*, *115*(G3), G03018. https://doi.org/10.1029/2009JG001191

Schindlbacher, A., Wunderlich, S., Borken, W., Kitzler, B., Zechmeister-Boltenstern, S., & Jandl, R. (2012). Soil respiration under climate change: Prolonged summer drought offsets soil warming effects. *Global Change Biology*, *18*(7), 2270–2279. https://doi.org/10.1111/j.1365-2486.2012.02696.x

Shangguan, W., Dai, Y., Duan, Q., Liu, B., & Yuan, H. (2014). A global soil data set for Earth system modeling. *Journal of Advances in Modeling Earth Systems*, *6*(1), 249–263. https://doi.org/10.1002/2013MS000293

Sitch, S., Friedlingstein, P., Gruber, N., Jones, S. D., Murray-Tortarolo, G., Ahlström, A., et al. (2015). Recent trends and drivers of regional sources and sinks of carbon dioxide. *Biogeosciences*, *12*(3), 653–679. https://doi.org/10.5194/bg-12-653-2015

Smith, J. E., Heath, L. S., & Patel, A. R. (2014). Forest carbon data for the 2008 U.S. forest national greenhouse gas inventory. https://doi.org/10.2737/RDS-2014-0032

Stockmann, U., Padarian, J., McBratney, A., Minasny, B., de Brogniez, D., Montanarella, L., et al. (2015). Global soil organic carbon assessment. *Global Food Security*, *6*, 9–16. https://doi.org/10.1016/j.gfs.2015.07.001

Tang, X., Fan, S., Du, M., Zhang, W., Gao, S., Liu, S., et al. (2020). Spatial and temporal patterns of global soil heterotrophic respiration in terrestrial ecosystems. *Earth System Science Data*, *12*(2), 1037–1051. https://doi.org/10.5194/essd-12-1037-2020

Tian, H., Lu, C., Yang, J., Banger, K., Huntzinger, D. N., Schwalm, C. R., et al. (2015). Global patterns and controls of soil organic carbon dynamics as simulated by multiple terrestrial biosphere models: Current status and future directions. *Global Biogeochemical Cycles*, *29*(6), 775–792. https://doi.org/10.1002/2014GB005021

Tifafi, M., Guenet, B., & Hatté, C. (2018). Large differences in global and regional total soil carbon stock estimates based on SoilGrids, HWSD, and NCSCD: Intercomparison and evaluation based on field data from USA, England, Wales, and France. *Global Biogeochemical Cycles*, *32*(1), 42–56. https://doi.org/10.1002/2017GB005678

Todd-Brown, K. E. O., Randerson, J. T., Hopkins, F., Arora, V., Hajima, T., Jones, C., et al. (2014). Changes in soil organic carbon storage predicted by Earth system models during the 21st century. *Biogeosciences*, *11*(8), 2341–2356. https://doi.org/10.5194/bg-11-2341-2014

Todd-Brown, K. E. O., Randerson, J. T., Post, W. M., Hoffman, F. M., Tarnocai, C., Schuur, E. A. G., & Allison, S. D. (2013). Causes of variation in soil carbon simulations from CMIP5 Earth system models and comparison with observations. *Biogeosciences*, *10*(3), 1717–1736. https://doi.org/10.5194/bg-10-1717-2013

van Groenigen, K. J., Qi, X., Osenberg, C. W., Luo, Y., & Hungate, B. A. (2014). Faster decomposition under increased atmospheric CO_2 limits soil carbon storage. *Science*, *344*(6183), 508–509. https://doi.org/10.1126/science.1249534

Wieder, W. R., Bonan, G. B., & Allison, S. D. (2013). Global soil carbon projections are improved by modelling microbial processes. *Nature Climate Change*, *3*(10), 909–912. https://doi.org/10.1038/nclimate1951

Wieder, W. R., Hartman, M. D., Sulman, B. N., Wang, Y. P., Koven, C. D., & Bonan, G. B. (2018). Carbon cycle confidence and uncertainty: Exploring variation among soil biogeochemical models. *Global Change Biology*, *24*(4), 1563–1579. https://doi.org/10.1111/gcb.13979

Wieder, W. R., Sulman, B. N., Hartman, M. D., Koven, C. D., & Bradford, M. A. (2019). Arctic soil governs whether climate change drives global losses or gains in soil carbon. *Geophysical Research Letters*, *46*, 1–10. https://doi.org/10.1029/2019GL085543

Wiesmeier, M., Urbanski, L., Hobley, E., Lang, B., von Lützow, M., Marin-Spiotta, E., et al. (2019). Soil organic carbon storage as a key function of soils—A review of drivers and indicators at various scales. *Geoderma*, *333*(November 2017), 149–162. https://doi.org/10.1016/j.geoderma.2018.07.026

Wu, Z., Dijkstra, P., Koch, G. W., Peñuelas, J., & Hungate, B. A. (2011). Responses of terrestrial ecosystems to temperature and precipitation change: A meta-analysis of experimental manipulation. *Global Change Biology*, *17*(2), 927–942. https://doi.org/10.1111/j.1365-2486.2010.02302.x

Zhao, X., Yang, Y., Shen, H., Geng, X., & Fang, J. (2019). Global soil-climate-biome diagram: Linking surface soil properties to climate and biota. *Biogeosciences*, *16*, 2857–2871. https://doi.org/10.5194/bg-2018-449

Ziegler, S. E., Benner, R., Billings, S. A., Edwards, K. A., Philben, M., Zhu, X., & Laganière, J. (2017). Climate warming can accelerate carbon fluxes without changing soil carbon stocks. *Frontiers in Earth Science*, *5*(February), 1–12. https://doi.org/10.3389/feart.2017.00002